470 Granville Street, Suite 630, Vancouver, BC V6C 1V5
Tel: 604-629-9075 | www.pecg.ca

Developments in the real-time detection of buried mineralization and geological structures using soil gas concentrations

Geoscience BC Report #
2022-12

Prepared For
Geoscience BC
April 1, 2022

R.E. Lett, Geochemist, Victoria, BC
D.A. Sacco, Palmer, Vancouver, BC
B. Elder, Palmer, Vancouver, BC
C.Knox, Palmer, BC

Abstract

Systematic changes observed in soil gas carbon dioxide and oxygen concentrations are influenced by the presence of faults and sulphides. Typically, there is an increase in the soil gas carbon dioxide concentration and a concomitant decrease in oxygen concentration above geological structures and sulphide mineralization. With increasing attention toward mineral exploration under cover and the necessity for effective mineral exploration methods in this setting, the development of a real-time, field-portable system for measuring soil-gas was initiated in 2019 and supported by Geoscience BC. A prototype soil gas measurement system was first tested at several sites in southwestern and central British Columbia. The testing demonstrated that the soil-gas composition over inferred faults has higher carbon dioxide concentrations and is more depleted in oxygen than over surrounding rocks. The soil gas measurement system was refined in 2020 and tested at Mount Milligan Cu-Au Mine where the location and nature of bedrock structures and mineralization are better understood. This report summarizes the initial system design and survey results and details the most recent testing at Mount Milligan Mine. The results from Mount Milligan show positive correlations of carbon dioxide and oxygen flux with geological structures and mineralization and provide a framework to design effective surveys using real-time soil gas measurements to support mineral exploration under cover.

Table of Contents

Abstract

1. Introduction 1
2. Background 3
3. Soil gas system and data acquisition 6
   - 3.1 Prototype system 6
   - 3.2 System Refinements 7
   - 3.3 Soil gas collection and measurement 8
4. Soil Gas Quality Control and Data Processing 10
5. Survey Results Summary from Prototype Testing 11
   - 5.1 Evaluation of Diurnal Variation 11
   - 5.2 System testing at the Leech River Complex, Jordan River, BC. 11
   - 5.3 Mouse Mountain and Shiko Lake Survey Results 13
6. Mount Milligan Survey 17
   - 6.1 Bedrock and Surficial Setting 17
   - 6.2 Survey Design and Data Collection 19
   - 6.3 Quality Control 19
   - 6.4 Mount Milligan Survey Results and Discussion 20
7. Conclusions and Recommendations 24
8. Acknowledgements 25
9. Certification 26
10. References 27

List of Figures

Figure 1. Location of the 2019 Jordan River, Mouse Mountain and Shiko Lake study areas (Lett et al. 2020) and the survey at Mount Milligan Mine completes in 2020 and 2021. 2

Figure 2. Flow chart depicting the mineralogical and biogeochemical processes that influence O_2 and CO_2 concentrations in soil gas (Modified from Hodges et al., 2019). Solid arrows represent flux from processes that occur under theoretical conditions of aerobic respiration balanced by the diffusion flow of gases (i.e., apparent respiratory

quotient [ARQ] = 1). Dotted arrows represent flux from processes that may induce a departure of the ARQ from unity. Numbers refer to reaction equations discussed in the text. 5

Figure 3. Prototype soil gas collection and analysis system. a) Sensor unit (25 by 22 by 11 cm); b) soil probe (1.5 m by 12.7 mm); c) pump and power source (25 by 12 by 16 cm); d) the soil gas collection and analysis system at a field site. 7

Figure 4. The modified soil gas collection-analysis system showing the sensor and shut-off valve unit, soil probe and lap top computer during the Mount Milligan survey. 8

Figure 5. An example of GasLab 2.1® software display from the temporal analysis of soil gas and atmosphere for CO_2 (blue line), O_2 (orange line) and temperature (red line) at Mouse Mountain. On the graph, sections A and C are measured in atmosphere and section B is measured in soil gas. The vertical grey lines on the graph roughly indicate an interval when gas flow is switched from atmosphere to soil gas and then from soil gas to atmosphere. In this example, a total of 32 measurements were made over a period of about five minutes. 9

Figure 6. Soil gas and atmospheric CO_2 measured in Victoria, BC, on August 10, 2019. 11

Figure 7. Results of the Leech River testing (Geology from Cui, et al., 2017; 2019 data version). Data displayed using proportional symbols. 13

Figure 8. Mouse Mountain geology, soil gas survey sites, ΔCO_2, ΔO_2 and $\Delta CO_2\&O_2$ values measured in soil gas. Data displayed using proportional symbols (* faults inferred from the $\Delta CO_2\&O_2$ results of this survey and simplified geology from Schimann, 2014). 14

Figure 9. East Zone, Shiko Lake geology, soil gas survey sites, and ΔCO_2, ΔO_2 and $\Delta CO_2\&O_2$ values measured in soil gas (Geology and fault locations from Lesage, 2011). 16

Figure 10. Soil gas measurement locations from the 2020 and 2021 surveys on the Mount Milligan Mine property (trench lithologies provided by Centerra Gold Services Inc.). 18

Figure 11. The variation of ΔCO_2 and $\Delta CO_2\&O_2$ in the soil gas at sites within a 20-m-wide buffer along the mapped bedrock trench. Trenching was completed after the soil gas measurements. 21

Figure 12. The variation of ΔCO_2 and the ΔO_2 (expressed as a negative) at sites within a 20-m-wide buffer along the mapped bedrock trench demonstrating the increase in CO_2 and concomitant reduction on O_2 associated with fractures. 21

Figure 13. Soil gas concentrations at the Mount Milligan Mine property. a) ΔCO_2, b) ΔO_2, c) $\Delta CO_2\&O_2$, and d) ΔCO_2 gridded to 10 m pixels based on the maximum of a three-cell search radius smoothed across a two-cell radius. Proportional dot plots are displayed based on progressive percentile breaks of 50, 75, 87, 93, 98 and 100. Gridded data symbolized using unequal bin percentile breaks of 30, 60, 80, 90, 95, 98, 99, 100. 23

List of Tables

Table 1. Mean and percent relative standard deviation (RSD%) of CO_2, number of measurements (N), pressure, temperature and humidity measured at 10-second intervals in atmospheric air and soil gas at Leech River Site 1. Two CO_2 measurement sequences were collected at this calibration site to test measurement reliability. Atmospheric air measurements occur before and after each soil gas determination to establish a CO_2 background concentration. 12

Table 2. Mean and percent relative standard deviation (RSD%) of O_2, pressure, temperature and humidity measured at 10-second intervals in atmospheric air and soil gas at Leech River Site 1. 12

Table 3. Precision of CO_2 and O_2 sensors indicated by percent relative standard deviation (RSD%). RSD% is calculated from repeated measurements over 10-second intervals

at individual sites and then averaged across all the sample sites to determine the overall precision of the survey. 19

Table 4. Summary statistics calculated from ΔCO_2, ΔO_2 and ΔCO_2&O_2 measurements from the Mount Milligan survey (O_2 measurements in soil gas at 14 sites where the sensor failed have been excluded from the summary statistics). 20

List of Appendices

Appendix A. Mount Milligan soil gas measurements

1. Introduction

Identifying and locating structures responsible for transporting mineralizing fluids is an important component of mineral exploration. Surface mapping, remote sensing and geophysical surveys can help, but locating these structures is considerably more difficult when buried beneath glacial sediments. Gases associated with mineral deposits and geological structures such as Rn, Hg, Methane (CH_4), carbon dioxide (CO_2) and Oxygen (O_2) can be detected in overlying sediments and used to facilitate exploration (*e.g.*, Gingrich, 1984; Rukhlov *et al.*, 2020).

In a review of past soil gas studies, Hale (2010) noted that the surveys either measured gas concentrations on-site (*e.g.*, Lovell *et al*., 1980) or collected a soil-gas sample for later analysis (*e.g.*, McCarthy *et al*., 1986, Hodges *et al*., 2019). While on-site analysis had the advantage of a real-time measurement, the commercial instrumentation used for analysis could be cumbersome and was historically expensive. The alternative requires gas capture, on-site storage, and transport to the lab for analysis, which increases the potential for contamination and would commonly involve a delay in the delivery of results. These factors have previously inhibited the utilization of soil gas in mineral exploration.

The availability of small, relatively inexpensive CO_2 and O_2 sensors and associated software, such as those distributed by CO2Meter Inc.™ (https://www.co2meter.com/) and Vernier Software and Technology, now provides an opportunity for devising an economical, on-site, real-time analytical system for measuring these gases. This report documents the development and testing of a portable system for measuring CO_2 and O_2 concentrations in soil designed to facilitate the detection of buried geological structures and mineralization. A summary is provided for the initial testing of the prototype system at an urban site in Victoria, British Columbia (BC), over a major fault near Jordan River, BC, and at Mouse Mountain and Shiko Lake, two drift-covered, porphyry Cu-Au disseminated, sulphide mineral occurrences with associated faults in central BC (Lett *et al.*., 2020) (Figure 1). The system was refined and deployed to Centerra Gold Services Inc.'s (Centerra) Mount Milligan property (Mount Milligan) in north-central British Columbia. A higher density survey was completed and direct observations of the bedrock from subsequent trenching provided the means to better gauge the efficacy of the system. The ultimate goal of this project is to provide a real-time method that can be used to guide mineral exploration activities and help focus detailed investigations such as targeting geophysics surveys, trenching and drilling programs.

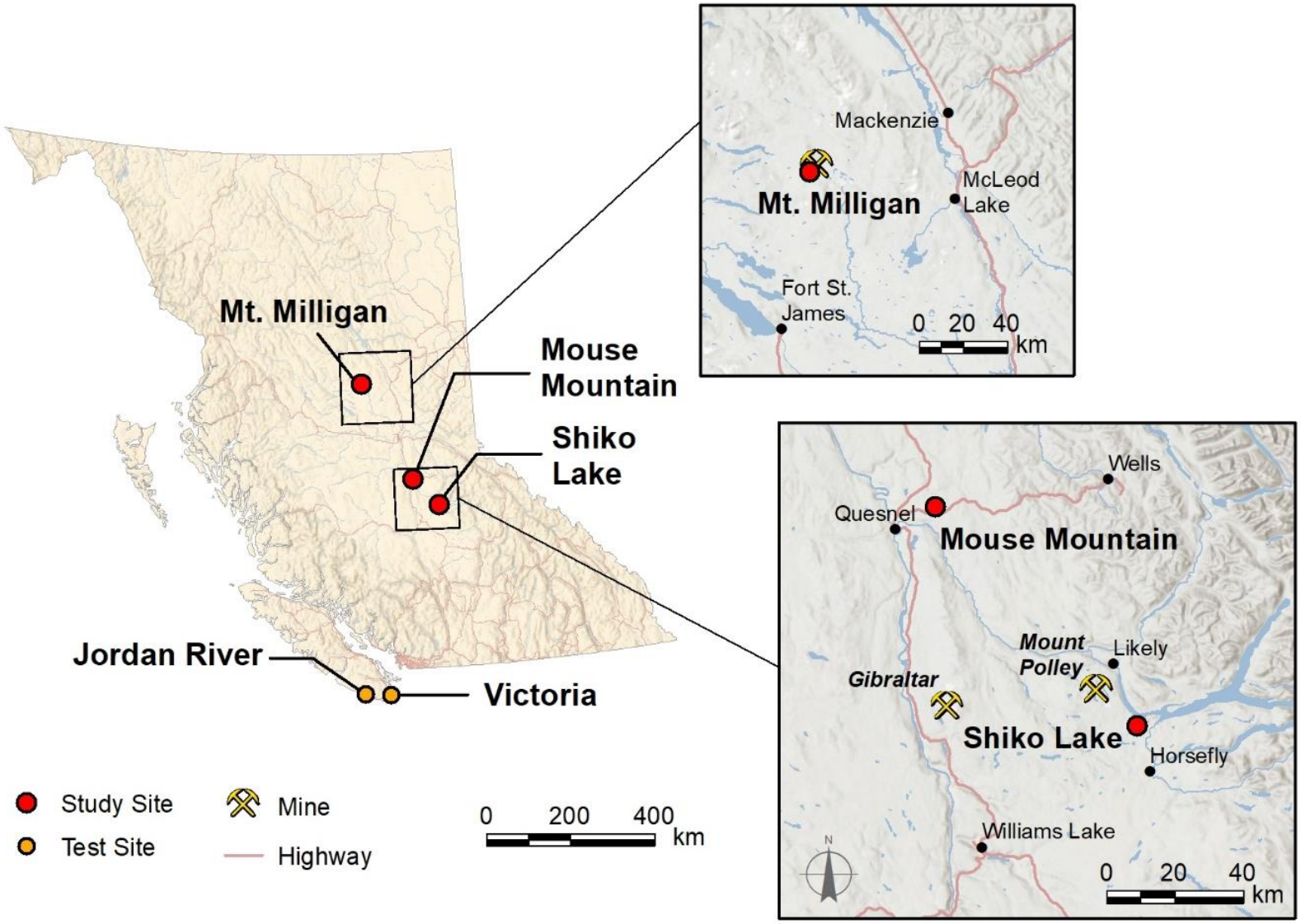

Figure 1. Location of the 2019 Jordan River, Mouse Mountain and Shiko Lake study areas (Lett et al. 2020) and the survey at Mount Milligan Mine completes in 2020 and 2021.

2. Background

There are many sources of gases in mineralized systems and fault structures are a conduit for volatile compounds and gases from deeper crustal rocks to the surface. Fridman (1990) distinguishes between the gases channeled by mineralized fault zones (*e.g.*, CO_2, H_2, hydrocarbons, ammonium (NH_4)), gases generated by mineral sulphide oxidation (*e.g.*, CO_2, hydrogen sulphide (H_2S), sulphur dioxide (SO_2), carbonyl sulphide (COS)), gases from metamorphic and hydrothermal reaction, and radiogenic gases. Superheated, saline, carbon dioxide-rich water is a key component of hydrothermal fluids (Robb, 2005), so many mineral deposits, including Archean-aged gold mineralized systems, have extensive carbonate alteration associated with major structures (Dubé *et al*., 2007). The reaction of carbonate alteration with acidic ground water could release CO_2 into faults and ultimately to the surface. Gold deposits are known to generate a variety of sulphur gases in addition to CO_2. For example, Kesler (1990) demonstrated through lab-controlled-weathering that shale-hosted, micro-sized gold ore released COS, carbon disulphide (CS_2), CH_4 and ethane (C_2H_6), and that the ratio of different gases helped distinguish between Au mineralized shale and barren rock.

Radon, He, Hg, CH_4 and CO_2 in soil gas and the near surface atmosphere have previously been used to identify faults and mineralization (*e.g.*, Gingrich, 1984; Rukhlov *et al*., 2020). Similarly, differences in CO_2 and O_2 concentrations in soil gas have revealed buried faults and mineral deposits. For example, Lovell *et al*. (1979, 1980, 1983) reported a decrease in O_2 and an increase in CO_2 in the soil gas sampled over fault hosted Pb-Zn sulphides beneath thick glacial deposits in Ireland. McCarthy *et al*. (1986) also found elevated CO_2 and CH_4 with decreased O_2 in soil gas samples collected from a depth of 0.5 m in overburden over the Crandon massive pyrite-sphalerite-galena deposit in Wisconsin, United States; a deposit buried beneath up to 65 m of glacial deposits. Even in the absence of sulphide mineralization faults are pathways for increasing gas flux from crustal rocks to the surface. Duddridge *et al*. (1991) observed increased CO_2 and decreased in O_2 concentrations in soil gas over faults at three glaciated sites in the United Kingdom.

The mineralogical and biogeochemical processes that likely influence the variation of O_2 and CO_2 concentrations in soil gas are depicted in Figure 2. Magmatic, hydrothermal and metamorphic processes active in the earth's deeper crust and upper mantle are the primary sources for CO_2. Lucic *et al*. (2014) found predominately magmatic CO_2 mixed with lesser amounts of biogenic and atmospheric CO_2 discharged from faults in the volcanically active Long Valley Caldera, USA. The products of thermally induced reactions between dolomite and quartz during the contact metamorphism of carbonate-rich crustal rocks are talc and CO_2 (Equation 1). Oxidation of mineral sulphides (*e.g.*, pyrite) by ground water in fractured and weathered rock generates sulphuric acid, which in turn can react with carbonate minerals (*e.g.*, calcite) to produce CO_2 (Equation 2; Equation 3). During oxidation–carbonate dissolution reactions, CO_2 will be generated while O_2 is consumed, hence increasing CO_2 and decreasing O_2 concentrations in soil gas (Equation 4). Conversely, silicate mineral weathering and the solution of carbonate minerals into ground water can remove CO_2 from the gas phase (Equation 5).

In addition to the geological contribution of CO_2 and O_2 to the soil environment, these gas concentrations are also affected by biogeochemical processes. Oxidation of organic matter and anaerobic respiration will deplete O_2 and increase CO_2 in soil gas (Equations 6, 7). Where the soil is close to bedrock, silicate minerals (*e.g.*, olivine) will remove CO_2 through weathering reactions. Hodges *et al*. (2019) propose an apparent respiratory quotient (ARQ) to explain how the variation of soil-gas CO_2 and O_2 responds to the balance

between gases produced by soil biochemical processes and gaseous diffusion in the soil environment (Figure 2). Ideally, when aerobic respiration, organic matter oxidation and diffusion are predominantly the control for CO_2 and O_2 in soil gas the ARQ is unity. However, if there are other processes and pathways contributing CO_2 into the soil (*e.g.*, silicate weathering), the ARQ is greater than unity. The soil biochemical processes can clearly influence the measured CO_2 and O_2 soil in the soil gas, and for this reason, samples are collected at a depth where these processes are minimized.

$$Dolomite - quartz\ reaction - 3CaMg\ (CO_2)_2 + 4SiO_2 + H_2O = Mg_3[(OH_2)Si_4O_{10}] + CaCO_3 + 3CO_2 \quad \{1\}$$

$$Pyrite\ oxidation - \ 4FeS_2 + 15O_2 + 8H_2O = 2Fe_2O_3 + 8H_2SO_4 \quad \{2\}$$

$$Calcite\ solution - \ CaCO_3 + H_2SO_4 = CaSO_4 + CO_2 + H_2O \quad \{3\}$$

$$Carbonate\ mineral\ solution - \ CaCO_3 + CO_2 + H_2O = Ca^{2+} + 2HCO_3 \quad \{4\}$$

$$Silicate\ weathering - (Ca, Mg)SiO_3 + CO_2 = (Ca, Mg)CO_3 + SiO_2 \quad \{5\}$$

$$Organic\ matter\ oxidation - \ CH_2O + O_2 = CO_2 + H_2O \quad \{6\}$$

$$Anaerobic\ respiration - \ CH_2O + 2MnO_2 + 4H^+ = CO_2 + 3H_2O + 2Mn^{2+} \quad \{7\}$$

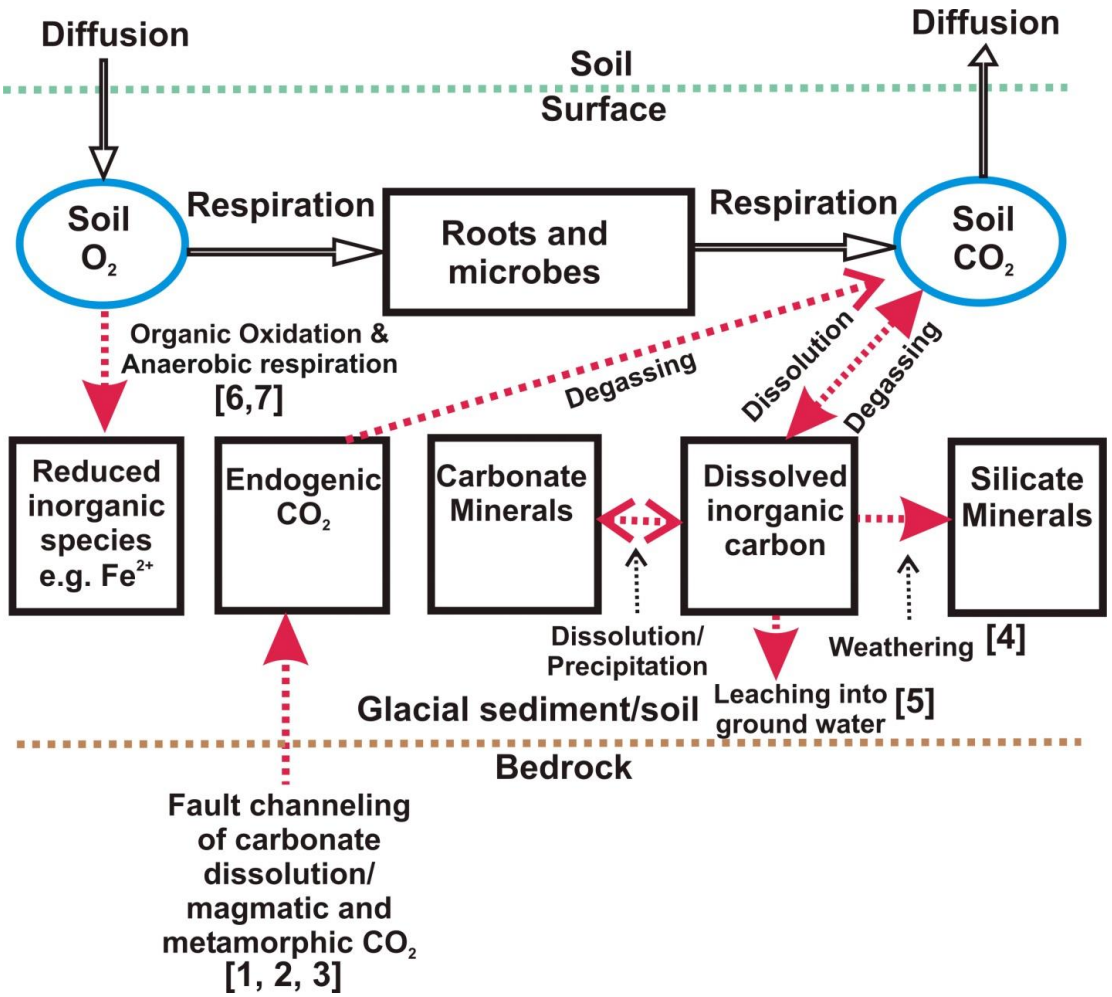

Figure 2. Flow chart depicting the mineralogical and biogeochemical processes that influence O_2 and CO_2 concentrations in soil gas (Modified from Hodges et al., 2019). Solid arrows represent flux from processes that occur under theoretical conditions of aerobic respiration balanced by the diffusion flow of gases (i.e., apparent respiratory quotient [ARQ] = 1). Dotted arrows represent flux from processes that may induce a departure of the ARQ from unity. Numbers refer to reaction equations discussed in the text.

3. Soil gas system and data acquisition

3.1 Prototype system

The prototype soil gas collection system for on-site analysis of CO_2 and O_2 was developed in 2019 (Figure 3). A summary of the system components is provided here, and a more detailed description is available in Lett, *et al*. (2020). The sensor unit, housed in a waterproof case, has a SprintIR®-6S 5% CO_2 Smart sensor and a UV Flux 25% Oxygen Smart Flow O_2 sensor mounted on a circuit board. The sensors measure CO_2 and O_2 concentration, barometric pressure, temperature and relative humidity. Each sensor body has an inlet and an exit port to attach flexible PVC tubes. One inlet port on the CO_2 sensor manifold is connected by a PVC tube to a corresponding exit port on the O2 sensor so that the gas can flow continuously into the two linked sensors. Each sensor circuit board is connected by USB cable to a computer equipped with CO2Meter.Inc GasLab 2.1 software.

The O_2 sensor inlet port is attached to a soil probe constructed from a hollow, 12.7 mm diameter, 1.5 m long steel tube fitted with a retractable, pointed tip. A steel hammer slides along the upper tube axis to drive the hollow-steel-tube 0.4 to 0.5 m into the overburden. The exit port on the CO_2 sensor is attached to a 6-volt, battery-powered diaphragm pump designed to continuously draw soil gas through the hollow-steel-tube sampler from overburden and into the sensors. Two shut-off valves, external to the sensor and pump unit, control the soil-gas flow from the hollow-steel-tube soil sampler to the sensors. By opening and closing the valves soil gas or atmospheric air, for calibrating the sensors with CO_2 and O_2, can be sampled independently.

Figure 3. Prototype soil gas collection and analysis system. a) Sensor unit (25 by 22 by 11 cm); b) soil probe (1.5 m by 12.7 mm); c) pump and power source (25 by 12 by 16 cm); d) the soil gas collection and analysis system at a field site.

3.2 System Refinements

Modifications to the 2019 prototype soil gas analysis system were largely to improve functionality in the field by minimizing the size and complexity of the components (Figure 9).

- The CO2 and O2 sensors and the diaphragm pump were integrated into a single waterproof case.
- The 6-volt battery was replaced by battery pack that holds four AA re-chargeable batteries and can be easily removed and replaced by a fully charged battery pack.
- The gas control valves that control the soil-gas flow from the hollow-steel-tube soil sampler to the sensors were reconfigured, connecting to a T-connector by Tygon® tubes, which was mounted on a rigid frame in a waterproof case. This shut-off valve unit reduced the number of connections and potential for contamination when alternating between soil gas and atmospheric air
- A longer soil gas probe was constructed to allow collection beneath thick organic soil or loose material at the surface, which also reduced the potential for atmospheric contamination.

Figure 4. The modified soil gas collection-analysis system showing the sensor and shut-off valve unit, soil probe and lap top computer during the Mount Milligan survey.

3.3 Soil gas collection and measurement

Ideally, a sample site is free of debris and the soil relatively dry, as excessive soil moisture can inhibit gas mobility. A study to determine the effects of soil moisture has not been completed, so saturated sites were avoided and sample collection was not completed during prolonged periods of rain. The site location coordinates were recorded by handheld GPS, the site photographed, and the soil probe, shut-off valve unit, sensor unit and the lap top computer assembled. Before collection, the system is primed using a small hand pump attached to the probe to ensure a continuous and stable gas flow through the probe and into the measurement system. The PVC tubing with hydrophobic in-line filter connects the inlet port on the O_2 sensor manifold in the sensor unit to the shut-off valve unit. Within the sensor unit the O_2 sensor manifold is connected by a tube to the CO_2 sensor manifold. A second tube on the CO_2 sensor manifold allows air or soil gas to exhaust to the atmosphere after measurement of CO_2 and O_2.

A pilot hole is created by hammering a solid, 12.7 mm diameter, pointed steel rod into the soil to approximately 30 cm depth, avoiding boulders or bedrock. The rod is extracted, examined for visible evidence of excess moisture, and replaced by the hollow soil probe, which is driven farther to 40–50 cm

depth. The hollow steel tube is then carefully withdrawn ~1 cm to open the retractable probe tip, so that soil gas can flow into the tube. Amundson and Davidson (1990) found that CO_2 in temperate soil profiles soil typically increases to a maximum at 0.4 m to 0.6 m depth where concentrations become constant. Their data suggest that 0.4 to 0.5 metres is an optimum and practical depth for routine soil gas collection.

PVC tubing is connected from the shut-off valve unit to the top of the hollow steel tube, the shut-off valve in the shut-off valve unit is closed, the shut-off valve to the atmosphere line is opened and the electric diaphragm pump in the sensor unit started. After connecting the sensors to the laptop computer with the USB cables, the GasLab 2.1 software is initiated. Individual sensor settings (sensor model number, computer port) are entered, and each sensor is calibrated by the GasLab 2.1 software to atmospheric levels (CO2 = 400 ppm, O2 = 209,050 ppm), as recommended by the manufacturer (CO2Meter Inc., 2015). The inlet to the atmospheric air PVC tube is positioned 3 m from the system and where possible clear of vegetation, to avoid possible human and plant influence on atmospheric measurements.

Atmospheric CO_2 and O_2 are measured at 10-second intervals, generally over a period of two minutes (section A in Figure 3), before the shut-off valve to the sensor unit is opened and the shut-off valve to the atmosphere closed. Measurements of soil CO_2 and O_2 concentrations continue at 10-second intervals for two minutes. Profiles of soil-gas measurements show that CO_2 levels typically increase to a plateau and O_2 levels decrease (section B in Figure 3). Finally, the shut-off valve to the atmosphere is opened, the valve to the sensor unit closed and measurements continued for two more minutes, to complete the measurement sequence (section C in Figure 3). The CO_2 and O_2 concentration, barometric pressure, temperature and relative humidity are captured by the software and recorded as a digital (.csv) text file. A full soil gas collection and measurement sequence can generally be completed in 20 minutes.

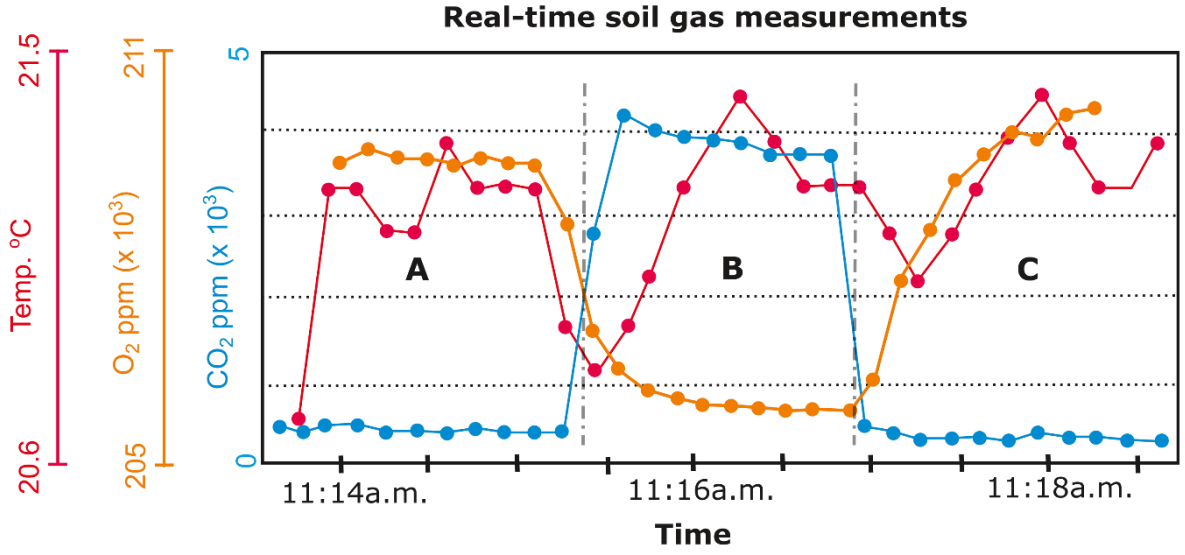

Figure 5. An example of GasLab 2.1® software display from the temporal analysis of soil gas and atmosphere for CO_2 (blue line), O_2 (orange line) and temperature (red line) at Mouse Mountain. On the graph, sections A and C are measured in atmosphere and section B is measured in soil gas. The vertical grey lines on the graph roughly indicate an interval when gas flow is switched from atmosphere to soil gas and then from soil gas to atmosphere. In this example, a total of 32 measurements were made over a period of about five minutes.

4. Soil Gas Quality Control and Data Processing

The CO_2 and O_2 concentrations are measured and recorded at 10-second intervals throughout the measurement sequence. The precision of the sensor measurements is determined from the raw CO_2 and O2 concentrations typically measured 10 to 15 times throughout the measurement sequence. These individual measurements are used to calculate a relative standard deviation (RSD%) value. An RSD% of 15% is considered good precision and between 15 and 30% acceptable precision (Fletcher, 1981). Combined sampling and sensor precision of CO_2 and O_2 soil gas is estimated using the coefficient of average variation (CV_{AVG} (%)) using the equation proposed by Abzalov (2008), which is calculated from duplicate measurements.

Soil gas concentrations are reported using the net soil-gas CO_2 (ΔCO_2) and O_2 (ΔO_2) values, which represent the difference between sensor-calibrated atmospheric gas concentrations and measured soil-gas concentrations (Equations 8 and 9). The atmospheric [1] and atmospheric [2] values in Equations 8 and 9 are mean values for the A and C datasets in Figure 5. The net ΔCO_2&O_2 concentration in soil gas (Equation 10) provides a single metric for the combined variation in CO_2 and O_2 concentrations of atmosphere and soil gases. Changes in individual CO_2 and O_2 concentrations can be associated with geological structures and mineralization, so all three metrics are evaluated.

$$\Delta CO_2 = soil\ gas\ CO_2 - \left[\frac{Atmosphere[1]\ mean\ CO_2 + Atmosphere\ [2]\ mean\ CO_2}{2}\right] \quad \{8\}$$

$$\Delta O_2 = soil\ gas\ O_2 - \left[\frac{Atmosphere[1]\ mean\ O_2 + Atmosphere\ [2]\ mean\ O_2}{2}\right] \quad \{9\}$$

$$soil\ gas\ \Delta CO_2 \& O_2 = \Delta CO_2 + \Delta O_2 \quad \{10\}$$

5. Survey Results Summary from Prototype Testing

5.1 Evaluation of Diurnal Variation

Diurnal fluctuations in atmospheric CO_2 and O_2 levels can complicate the interpretation of soil gas measurements, so the diurnal variation was evaluated on August 10, 2019 in Victoria, BC (Figure 2). Atmospheric and soil gas CO_2 and O_2 concentrations were measured every 2 to 3 hours between 9:00 and 22:00 hour, which revealed that CO_2 and O_2 decrease during the day and increase in the evening (Figure 6). The average CO_2 variation between 9:00 and 16:45 hrs is 200 ppm. Based on the pattern of CO_2 and O_2 the optimum time for measuring soil gas during a day is between 9:00 hrs and 16.45 hrs.

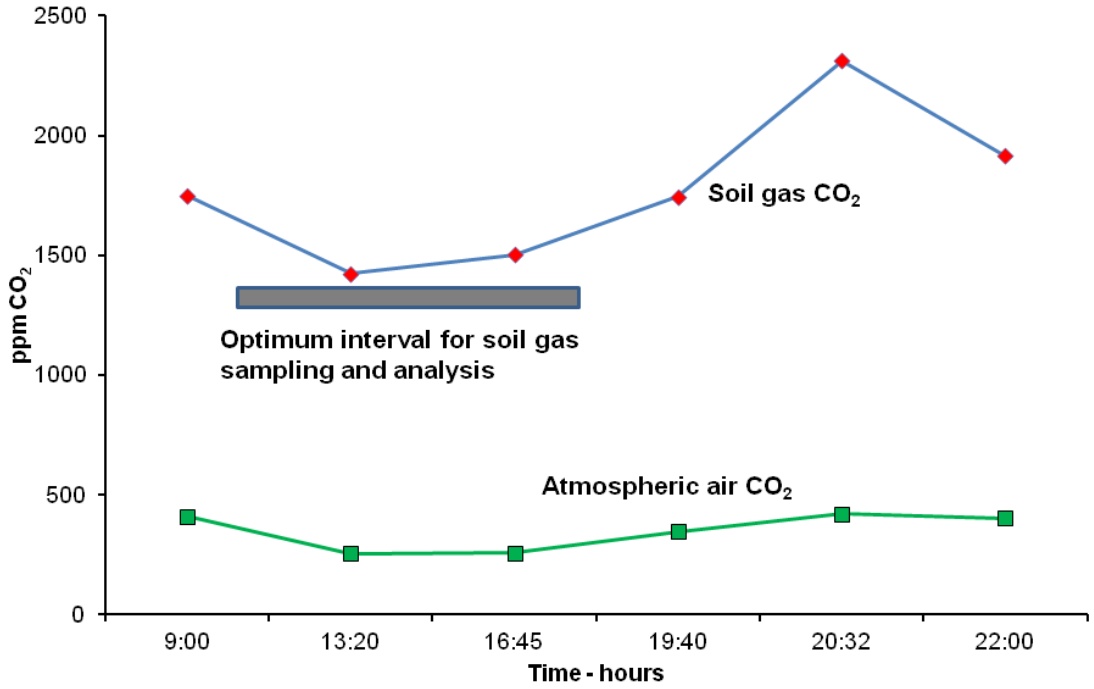

Figure 6. Soil gas and atmospheric CO_2 measured in Victoria, BC, on August 10, 2019.

5.2 System testing at the Leech River Complex, Jordan River, BC.

The reliability and functionality of the prototype system was assessed by measuring CO_2 and O_2 soil gas concentrations across the Leech River Fault Zone, 12 km north of Jordan River, BC (Figure 1). The Leech River fault zone, comprising several sub-parallel normal- and thrust faults, marks the contact between basalt of Eocene Metchosin Igneous Complex to the south and the variably metamorphosed and deformed metasedimentary rocks of the Leech River Complex to the North.

Carbon dioxide and O_2 concentrations, pressure, temperature and humidity were measured in the soil gas at five sites with the prototype system along a 6 km section of logging road (Figure 7). The mean and RSD% values of CO_2 and O_2 at site 1 are listed in Tables 1 and 2, respectively.

Table 1. Mean and percent relative standard deviation (RSD%) of CO_2, number of measurements (N), pressure, temperature and humidity measured at 10-second intervals in atmospheric air and soil gas at Leech River Site 1. Two CO_2 measurement sequences were collected at this calibration site to test measurement reliability. Atmospheric air measurements occur before and after each soil gas determination to establish a CO_2 background concentration.

Measurement	N	CO_2 ppm	CO_2 RSD%	Pressure mbar	Pressure RSD%	Temp. °C	Temp. RSD%	Humidity %	Humidity RSD%
Mean atmospheric air 1	10	416.4	7.1	941.7	0.4	22.3	1.5	41.5	2.5
Mean soil gas 1	13	9452.3	4.2	940.7	0.1	21.7	1.8	42.1	3.4
Mean atmospheric air 2	11	519.1	21.8	940.5	0.1	21.3	1.2	42.3	2.4
Mean soil gas 2	12	9487.7	16.4	939.6	0.1	20.8	2.4	42.9	4.6
Mean atmospheric air 3	14	569.2	7.4	939.5	0.1	20.8	2.1	44.9	1.5

Table 2. Mean and percent relative standard deviation (RSD%) of O_2, pressure, temperature and humidity measured at 10-second intervals in atmospheric air and soil gas at Leech River Site 1.

Measurement	N	O_2 ppm	O_2 RSD%	Pressure mbar	Pressure RSD%	Temp. °C	Temp RSD%	Humidity %	Humidity RSD%
Mean atmospheric air 1	17	206826	0.7	911.8	0.2	20.4	0.7	44.4	3.6
Mean soil gas 1	13	197410	0.5	907.2	0.2	20.7	0.3	46.8	3.6
Mean atmospheric air 2	14	204645	0.3	913.4	0.1	20.8	0.2	48.8	2.7

The RSD% values for most CO_2, O_2, pressure, temperature and humidity measurements are small, and therefore, survey results have good precision (*i.e.*, RSD < 15%). The exception is the RSD% of 22 for the second atmospheric air measurement and RSD% of 16 for the second soil gas measurement, affected by a spike of several increasing CO_2 measurements during a change from atmosphere to soil gas. These values likely indicate the mixing of soil gas and atmosphere during the change. Results from the first field test of the system found up to 1.73% ΔCO_2&O_2 in soil gas close to the fault with lower concentration in samples from sites to the south.

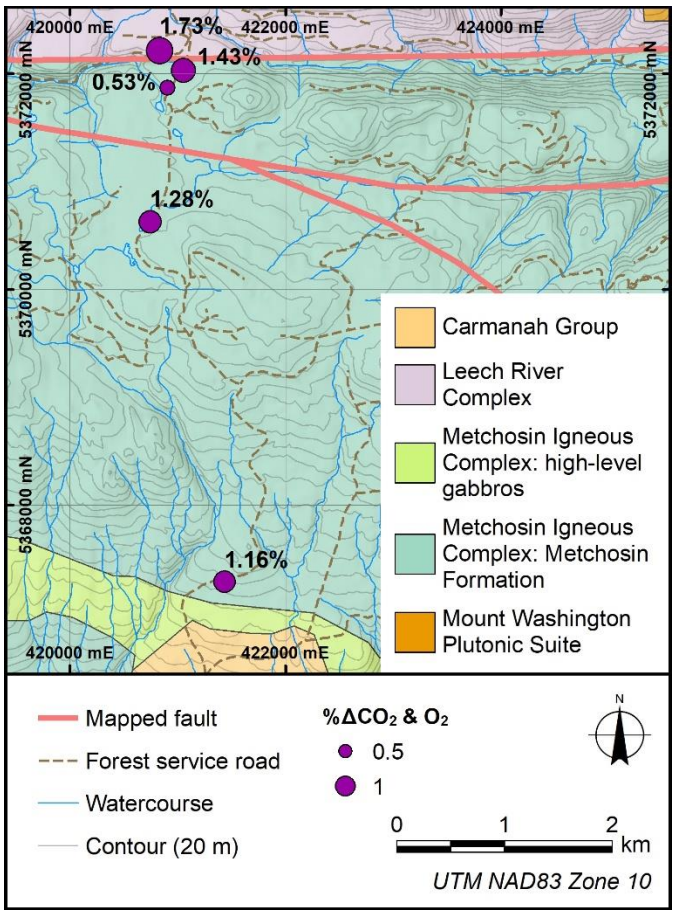

Figure 7. Results of the Leech River testing (Geology from Cui, et al., 2017; 2019 data version). Data displayed using proportional symbols.

5.3 Mouse Mountain and Shiko Lake Survey Results

Upon satisfactory system testing, two field locations were chosen in central BC based on the occurrence of faults in existing maps, Cu-Au porphyry-style disseminated sulphide mineralization and a cover of glacial drift: 1) Mouse Mountain (MINFILE 093G 003; BC Geological Survey, 2019) mineral occurrence, 13 km east of Quesnel; and 2) the Shiko Lake property (MINFILE 093A 058), 17 km north of Horsefly (Figure 1).

At Mouse Mountain, soil gas and soil were sampled at 33 sites along three transects crossing an area south the Valentine Cu-Au porphyry–style sulphide mineralized zone (Figure 8). The Valentine zone has disseminated chalcopyrite, pyrite, bornite, magnetite and malachite associated with Jurassic calc-alkaline plutons intruded into Upper Triassic to Lower Jurassic Nicola Group potassic altered, sedimentary and volcanic rocks (Jonnes and Logan, 2007). The rocks have been fractured and faulted (Schimann, 2014), but exact location of a northeast-southwest-trending fault crossing the area south of the Valentine zone is uncertain (Figure 8). While the fault is shown on past geological maps as transecting the monzonite, Jonnes and Logan (2007) found no outcrop evidence for the structure. Since the fault structure is drawn on the most recent geological map of the Mouse Mountain property, it is shown as a guide for interpreting the geochemistry and identified as "mapped" in figures. While bedrock is exposed at the Valentine zone it is concealed to the south beneath a till veneer and mainly Brunisolic soil.

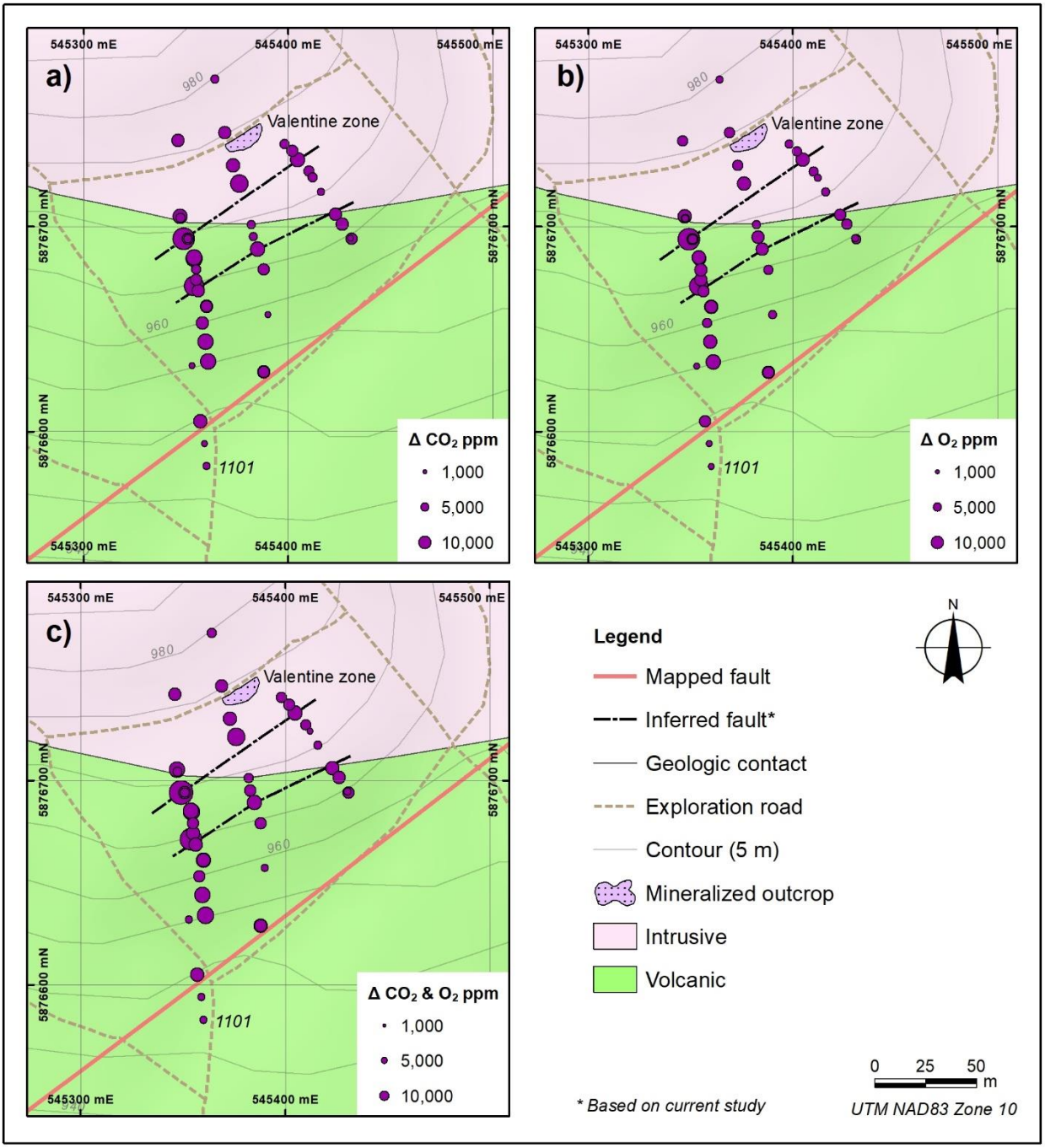

Figure 8. Mouse Mountain geology, soil gas survey sites, ΔCO₂, ΔO₂ and ΔCO₂&O₂ values measured in soil gas. Data displayed using proportional symbols (* faults inferred from the ΔCO₂&O₂ results of this survey and simplified geology from Schimann, 2014).

At Mouse Mountain, the southernmost $\Delta CO_2\&O_2$ value in soil gas (site 1101), measured over the previously mapped northeast-southwest fault was very low (Figure 10a), suggesting an absence of structural influence on the soil gas concentrations. Measurements 50 m north of the mapped fault on the same transect, however, detected $\Delta CO_2\&O_2$ values up to 50 000 ppm. It is known that the location of the fault is poorly

constrained, and the real-time measurements suggested the fault system is farther north, thus more closely spaced samples were taken in that area to ensure that the structure was not missed by the survey.

The highest $\Delta CO_2\&O_2$ soil gas values occur along the westernmost transect (Figure 8). From these peaks, $\Delta CO_2\&O_2$ values between up to 28 000 ppm extend along northeast linear trends across the three transects (Figure 8c). These results suggest the occurrence of a concealed fault or fracture system north of the fault location mapped by Schimann (2014). Black dashed lines on Figure 8 estimate the location of structural features as indicated by the soil-gas measurements and are referred to as inferred faults.

Analysis of B-horizon soil samples for pH and trace elements by a water leach followed by inductively coupled plasma mass/emission spectrometry show a spatial association between the soil gas anomalies and soil sulphur chemistry (Lett *et al*., 2020). Inverse difference hydrogen factor (Smee, 1998, 2003) values, calculated from soil pH, are also related to soil gas $\Delta CO_2\&O_2$ anomalies reflecting the impact of a higher CO_2 flux from bedrock on soil chemistry. Increased water-soluble sulphur detected in the soil and spatially associated with the $\Delta CO_2\&O_2$ anomalies could reflect sulphur gases such as carbonyl sulphide from oxidizing sulphides (Hale, 2010).

A diorite-syenite-monzonite stock with associated sulphide mineralization intrudes Nicola Group basaltic and andesitic rocks on the Shiko Lake Cu-Au porphyry property (Morton, 2003; Lesage, 2011). Soil gas and soil sampling were carried out over the Quarry and East mineralized zones. Only the East zone is discussed here because the there is no known reported structures at the Quarry zone, whereas faults have been identified at the East Zone (Lett *et al*., 2020).

At the East zone, northeast-striking faults cutting the andesite are partially covered by till and soil (Figure 9). Soil gas and soil, sampled from seven sites on the East zones reveal anomalous soil gas $\Delta CO_2\&O_2$ and elevated water extractable sulphur values in the soil close to a northeast striking fault. While the $\Delta CO_2\&O_2$ and IDH anomalies are proximal to the mapped fault, the trace metal soil anomalies are generally farther north suggesting that they reflect clastic transport of mineralized bedrock in till (Lett *et al*., 2020).

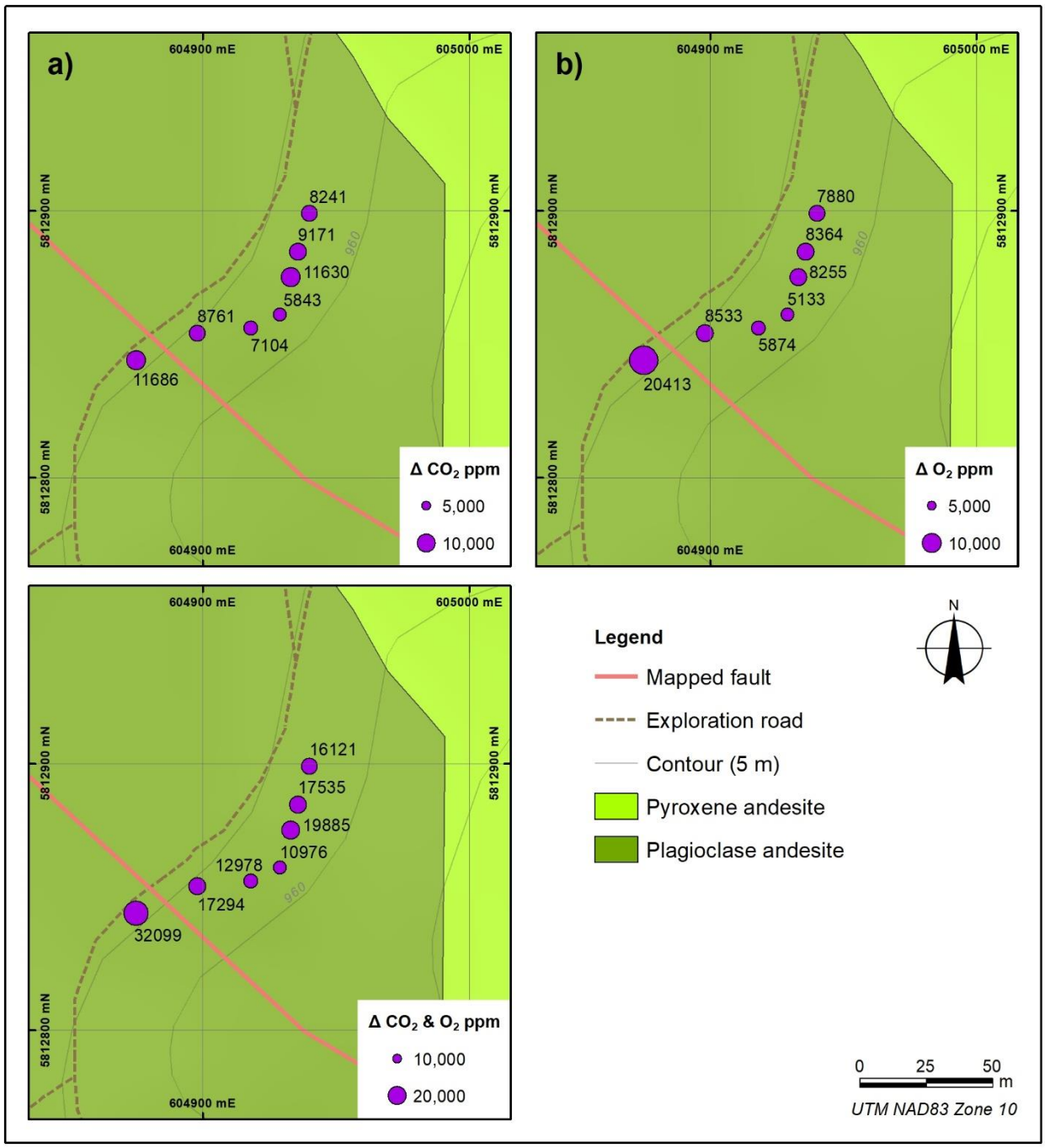

Figure 9. East Zone, Shiko Lake geology, soil gas survey sites, and ΔCO_2, ΔO_2 and ΔCO_2&O_2 values measured in soil gas (Geology and fault locations from Lesage, 2011).

6. Mount Milligan Survey

The initial testing at Mouse Mountain and Shiko Lake yielded positive results. It was recognized, however, that the locations of the structures and mineralization were not understood sufficiently well to adequately determine the spatial relationship between the soil gas anomalies and the geologic features. In addition, the understanding of the surficial geology at the previous testing sites was limited, and therefore, its influence on the soil gas concentrations could not be considered in the data evaluation. Centerra provided access to the Mount Milligan Property to complete additional testing that could be corroborated with detailed descriptions of the bedrock and surficial geology. The survey consisted of CO_2 and O_2 measurements at 163 sites and was carried out over 10 days.

6.1 Bedrock and Surficial Setting

The Mount Milligan property is located within the Quesnel terrane in central BC (Figure 1). Fitzgerald *et al*. (2020) have described the geology and mineralization of the Cu-Au porphyry deposit. The survey area is within the Upper Triassic andesitic volcanic rocks of the Witch Lake succession (Logan *et al*., 2010). Observations provided by Centerra from a trench parallel to one of the soil gas survey transects indicate that the geology is more complex, consisting of monzonite dykes intruded into andesite flows and andesite tuffs with several fracture zones and veins (Figure 10). Disseminated pyrite is common in these rocks and some fracture zones have chalcopyrite. In addition, two fault traces are projected within the survey area (Figure 10). The location and configuration of these faults at surface is approximated from measurements in drill core.

The survey area is mantled by subglacial till that was deposited by east-northeastward flowing ice. The land surface slopes gently to the east. Bedrock is exposed roughly 150 m to the west of the survey grid and outcrops occur sporadically in the western part of the grid. Till thickness generally increases to the east. Measurements were collected from an area interpreted as a veneer (*i.e.*, <2 m thick), but pockets of thicker material occur locally throughout the survey area. Till is highly compacted and generally composed of a sandy-silt matrix containing angular to subrounded pebbles, cobbles and boulders. Till was locally reworked by meltwater on the eastern side of the survey area, generally resulting in a thin veneer (20-50 cm) of sandy diamict at the surface. Bruisolic soils developed on the till commonly include L-F-H soil horizons greater than 15 cm thick and mainly support immature pine and fir forest.

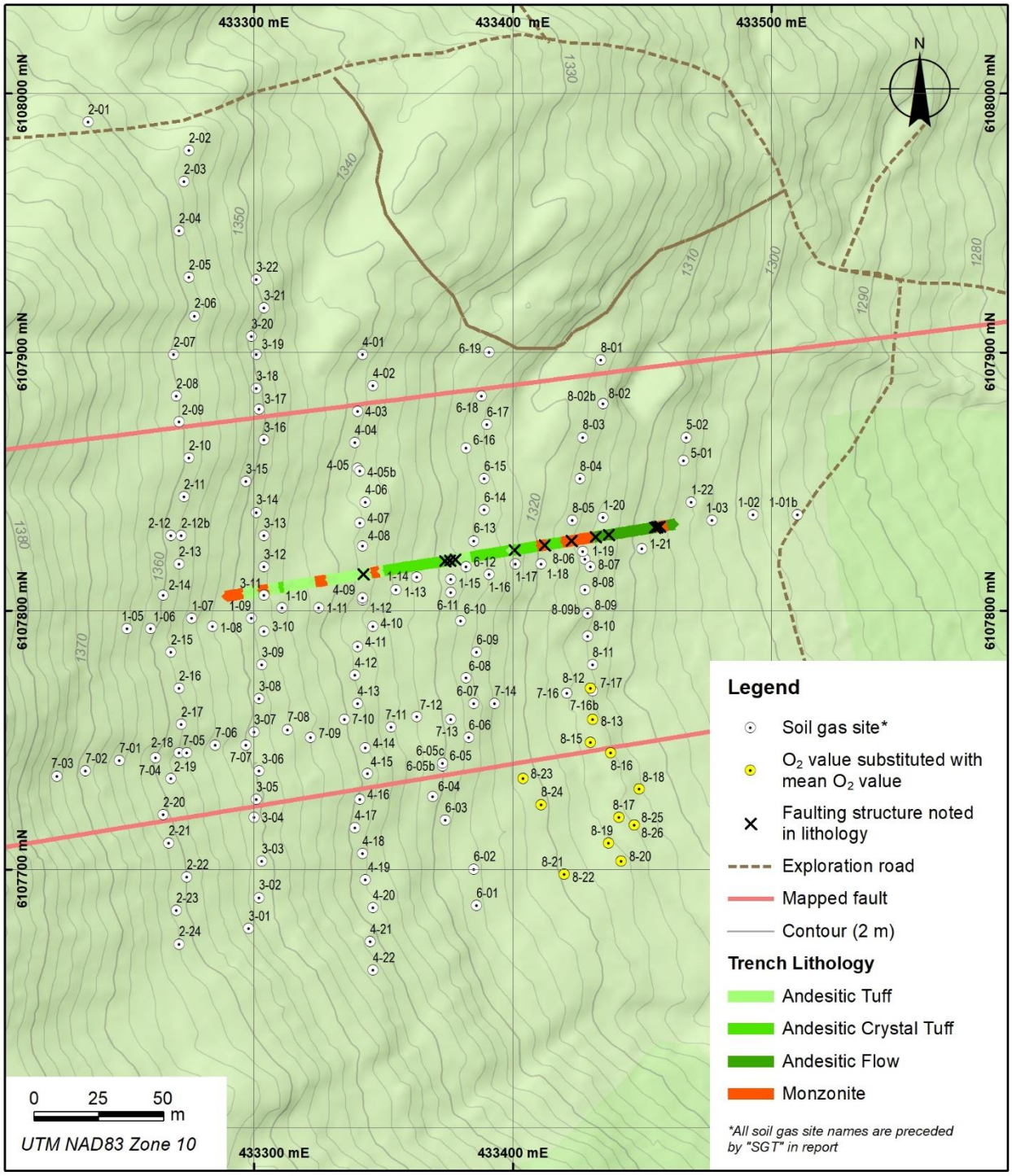

Figure 10. Soil gas measurement locations from the 2020 and 2021 surveys on the Mount Milligan Mine property (trench lithologies provided by Centerra Gold Services Inc.).

6.2 Survey Design and Data Collection

The soil gas survey was designed to coincide with the fault trace projections and the planned trenching program. Soil gas measurement sites were predetermined at 10 m intervals along north-south and southwest-northeast oriented transects. The north-south transects cross the projected fault trace while the southwest-northeast lines parallel the proposed trench locations. Actual soil gas measurement locations were adjusted from the predetermined plan based on ground conditions. Areas of poor drainage, increased boulder or cobble presence and thick vegetations were avoided.

Two soil gas collection-measurement campaigns were carried out at Mount Milligan. During a first attempt in October 2020, CO_2 and O_2 were measured at nine sites before the survey was suspended due to a snow and water-saturated overburden. A second campaign in July 2021 measured CO_2 and O_2 in the soil gas at 154 sites. The site locations and station numbers are shown on Figure 10.

Soil gas measurements followed the collection procedures described in section 3.3. In general, the soil gas measurements were completed with few complications and within 20 minutes. At some locations, setting up the system for measurements required extra time because it was difficult to drive the probe into the ground or ensure a good seal. Both scenarios were due to increased clast contents in the surface materials and were most common on the western side of the survey where drift is the thinnest.

An O_2 sensor malfunctioned in the survey and as a result 14 of the sites do not have O_2 concentration measurements (Figure 9). The mean ΔO_2 value from the entire survey was used to calculate ΔCO_2&O_2 values for the fourteen sample sites affected by the sensor malfunction.

6.3 Quality Control

Carbon dioxide and O_2 data generated from the air and soil gas analyses at each site were used to calculate the individual sensor measured mean, standard deviation and precision expressed as RSD%. An overall mean and an overall RSD% determined from the individual sensor statistics are listed in Table 3. An overall precision of +/- 17.4% for soil gas CO_2 at a mean concentration of 3068 ppm is within an acceptable precision range (+/- 15 to 30%). Overall precision of the soil air at 388 ppm is better at 10.5%. The excellent overall O_2 sensor precision of +/- 0.76% reflects the large overall mean O_2 concentration of 204619 ppm.

Table 3. Precision of CO_2 and O_2 sensors indicated by percent relative standard deviation (RSD%). RSD% is calculated from repeated measurements over 10-second intervals at individual sites and then averaged across all the sample sites to determine the overall precision of the survey.

Statistic	Value (ppm)	Relative standard deviation (RSD%)
Mean soil gas CO_2	3068 ppm	17.4
Mean soil gas O_2	204619 ppm	0.76
Mean air CO_2	388 ppm	10.5

Measurement precision expressed as an average coefficient of variation, CV_{AVG} was calculated using the ΔCO_2 and ΔO_2 values from eight sites where there were duplicate soil gas measurements. At each

duplicated site, atmospheric air and soil gas was measured with the system at two adjacent locations within 1 m of each other. The CV_{AVG} are 30.3% for ΔCO_2, 29.2% for ΔO_2 and 26.6% for $\Delta CO_2\&O_2$. These values reveal a greater variability compared to precision estimated from the prototype testing, which were 18.4% for ΔCO_2, 14.0% for ΔO_2, and 15.9% for $\Delta CO_2\&O_2$. The values are, however, still within the 15 to 30 CV_{AVG} considered to be an acceptable level of precision (Abzalov, 2008). The greater variability in the Mount Milligan data is attributed to the difficulty attaining a tight seal between the probe and the soil, which may be related to the lower consolidation of the reworked till and higher clast contents in the shallower till deposits.

6.4 Mount Milligan Survey Results and Discussion

The summary statistics for ΔCO_2, ΔO_2 and $\Delta CO_2\&O_2$ in soil gas are listed in Table 4. In general, the data shows good contrast with relatively normally distributed data. As such, standard percentiles should accurately depict anomalies in proportional dot plots.

Table 4. Summary statistics calculated from ΔCO_2, ΔO_2 and $\Delta CO_2\&O_2$ measurements from the Mount Milligan survey (O_2 measurements in soil gas at 14 sites where the sensor failed have been excluded from the summary statistics).

Statistic	ΔCO_2 ppm	ΔO_2 ppm	$\Delta CO_2\&O_2$ ppm
Number of measurements	142	128	128
Minimum	570	395	1396
Mean	2301	2418	4720
Median	2076	2281	4388
Standard deviation	1198	1039	2030
80^{th} percentile	3034	3144	6125
90^{th} percentile	3708	3684	7140
95^{th} percentile	4276	4304	8299
98^{th} percentile	4788	5166	8955
Maximum	19184	5906	21602

Carbon dioxide and O_2 measured in soil gas at sites within a 20-m-wide buffer of the trench were compared to the trench logging results (Figures 11 and 12). Several intervals of fracturing and veining are reported including a zone of intense fractures towards the eastern end of the trench (~150-175 m on Figures 11 and 12). This zone corresponds to sample sites with soil gas ΔCO_2 values over 4000 ppm and $\Delta CO_2\&O_2$ values over 8000 ppm, which are both around the 90th percentile of the dataset. Identified fracturing and/or veining at 67 m, 101 m, and ~125-150 m along the trench is also spatially correlative with ΔCO_2 and $\Delta CO_2\&O_2$ peaks in soil gas. These results indicate that there is a measurable correlation between fractures, veining, ΔCO_2 and $\Delta CO_2\&O_2$. Depletion of O_2 with concomitant CO_2 increases (Figure 12) suggest sulphide mineralized in some fractured areas, specifically at 175 m.

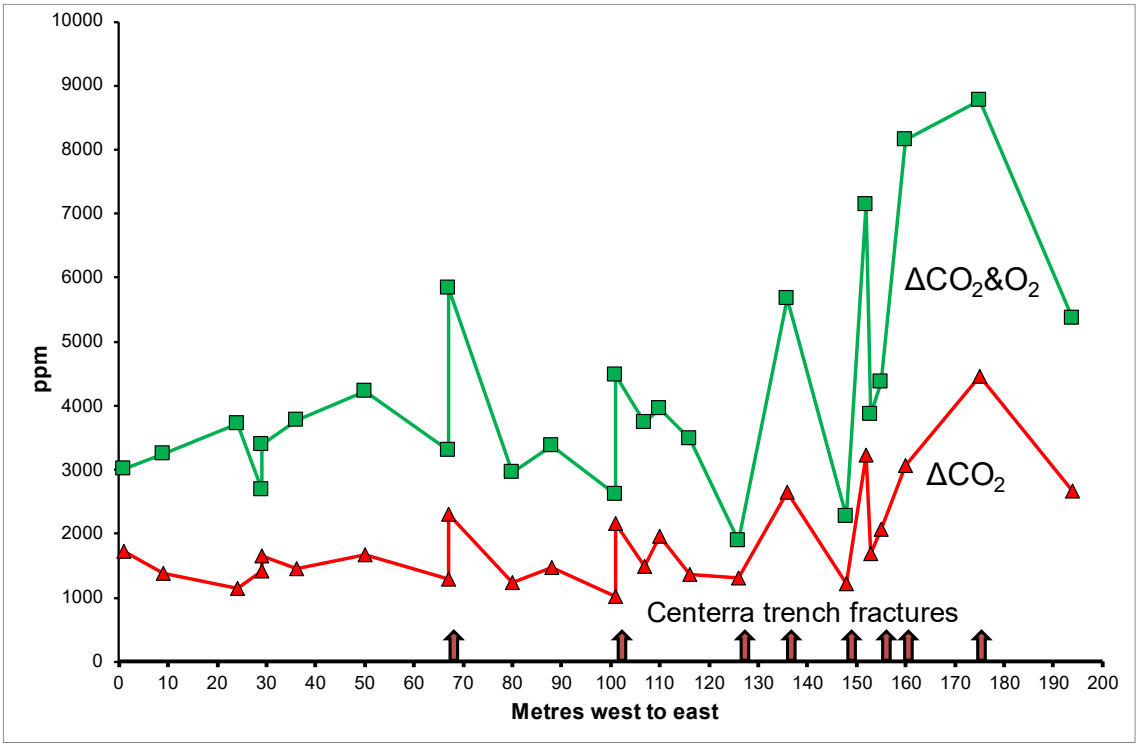

Figure 11. The variation of ΔCO_2 and ΔCO_2&O_2 in the soil gas at sites within a 20-m-wide buffer along the mapped bedrock trench. Trenching was completed after the soil gas measurements.

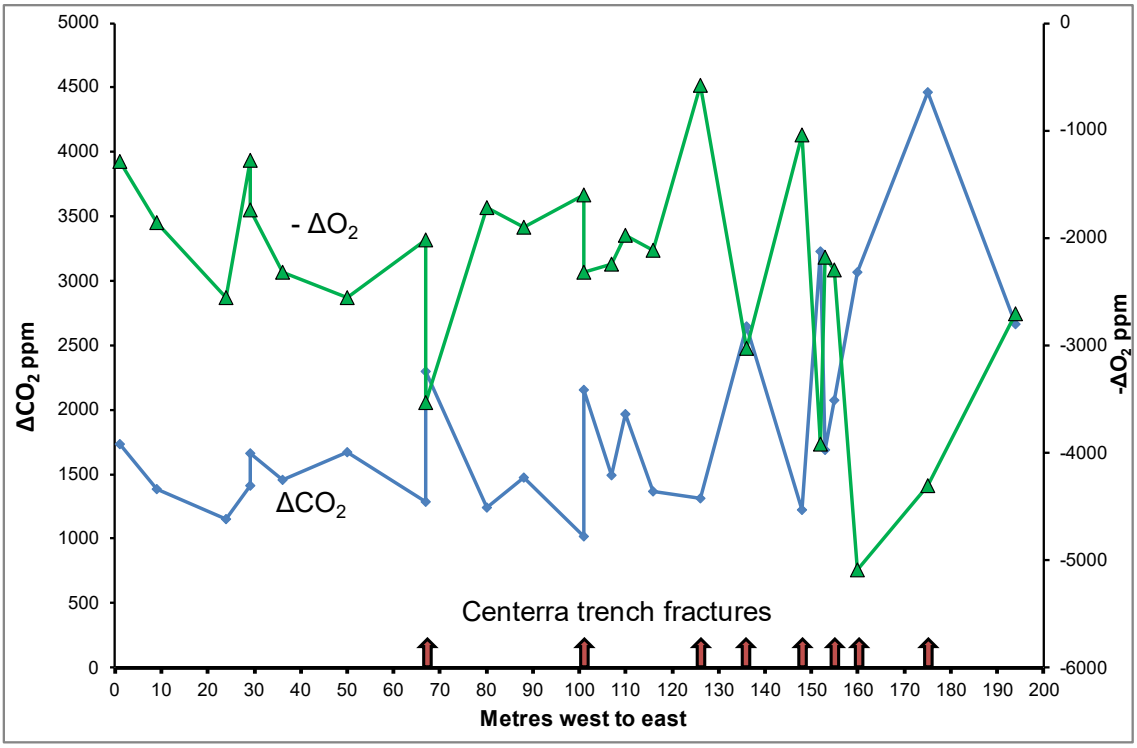

Figure 12. The variation of ΔCO_2 and the ΔO_2 (expressed as a negative) at sites within a 20-m-wide buffer along the mapped bedrock trench demonstrating the increase in CO_2 and concomitant reduction on O_2 associated with fractures.

Several patterns are apparent in the ΔCO_2, ΔO_2, and $\Delta CO_2\&O_2$ measurements over the entire survey area (Figure 13). The highest values for all metrics cluster in the southern part of the survey area. There is a linear trend oriented roughly southwest-northeast that could be associated with the southern fault, which is projected to intersect the surface in the same region, albeit at a different orientation. The location of this fault is projected to a flat surface from measurements in drill core, so it is possible that the soil gas measurements represent a more accurate indication of the fault trace. The highest ΔCO_2, ΔO_2, and $\Delta CO_2\&O_2$ values cluster in the east and southeast parts of the survey area. The O_2 sensor failure occurred in the southeast corner, so there is some additional error associated with the $\Delta CO_2\&O_2$ data; however, the ΔCO_2 is highly anomalous and considered reliable. A possible interpretation of the data from the southern part of the survey is they represent a linear structure that has a concentration of mineralization on the eastern extent. This is supported by the trench data that indicates increased concentrations of fracturing toward the east.

The projected trace of the northern fault is somewhat coincident with several very faint soil gas anomalies, but there is no clear association. This could mean that the projected fault trace is incorrect, and the actual location is beyond the survey. Alternatively, it could mean there is less CO_2 associated with this fault and the signal is masked by the higher concentrations to the south. It is also possible that the fault fractures are sealed with clay alteration and gas flow is inhibited.

As discussed in Section 2, soil gas anomalies could also reflect increased soil moisture, biological activity and landscape variation (Hodges *et al*., 2019). Variance along the depth profiles of CO_2 and O_2 concentrations may also contribute to the observed variation in the measured soil gas concentrations (Amundson and Davidson, 1990). Increased moisture was noted at the surface of some sample sites in the southeast part of the survey, but the soil was recorded as dry, so moisture is not considered to have significantly influenced the measured soil gas concentrations. All measurements were collected at a similar depth; however, the composition of the soil may affect the soil gas concentration profiles. At some locations, especially where the surface material was loose, variation of soil gas CO_2 and O_2 with depth may have influenced the results.

While the highest ΔCO_2 value of 1.9% measured during the Mount Milligan survey is lower than the maximum 6.1% CO_2 in soil gas measured in Ireland (Lovell *et al*., 1980), the linear patterns and correlations with confirmed structures suggest the anomalies identified in this survey can be attributed to geological sources. The results of this case study indicate that the 10-m sample spacing adequately defines anomalous areas. This measurement density may be required to identify specific fault traces; however, it appears that highly anomalous areas, potentially associated with increased sulphide concentrations, can be sampled at a lower density, and still be identified in the survey results. The survey design of linear transects perpendicular to the target structures worked well for this survey. If surveys are intended to identify non-linear features (*e.g.*, zones of mineralization), a grid-based approach may be more suitable.

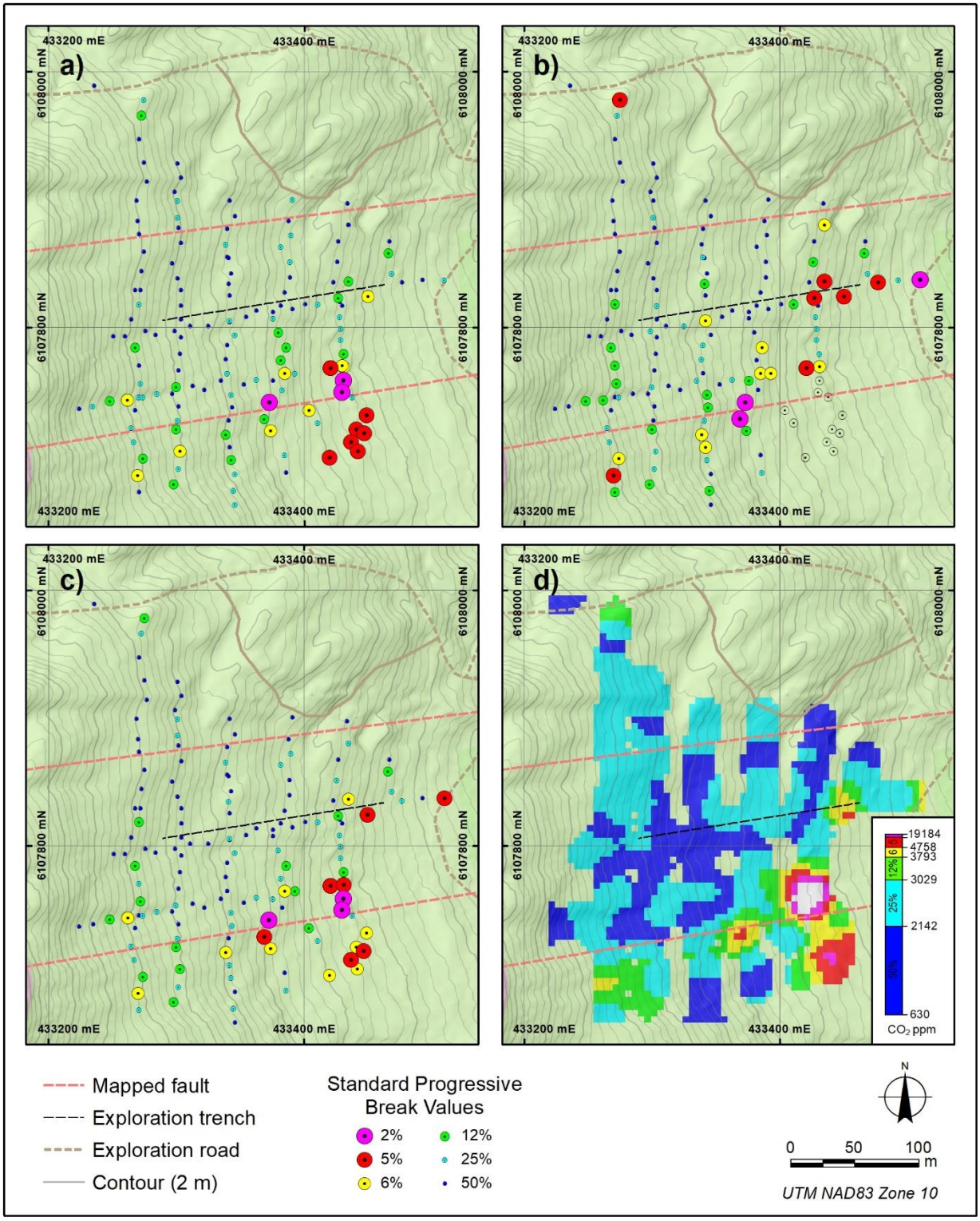

Figure 13. Soil gas concentrations at the Mount Milligan Mine property. a) ΔCO_2, b) ΔO_2, c) ΔCO_2&O_2, and d) ΔCO_2 gridded to 10 m pixels based on the maximum of a three-cell search radius smoothed across a two-cell radius. Proportional dot plots are displayed based on progressive percentile breaks of 50, 75, 87, 93, 98 and 100. Gridded data symbolized using unequal bin percentile breaks of 30, 60, 80, 90, 95, 98, 99, 100.

7. Conclusions and Recommendations

A real-time CO_2 and O_2 soil gas measurement system intended to detect geological faults and related mineralization under glacial deposits has been designed and tested at several sites in central and southern British Columbia. A prototype unit was used to demonstrate that commercial electronic gas sensors can be used in conjunction with specialized software to reliably measure and record real-time atmospheric air and soil gas CO_2 and O_2 concentrations. It was also determined that diurnal variation in gas concentrations do not compromise soil gas survey results provided that the measurements are completed between 09:00 and 16:45 hours. The system was tested at the Mouse Mountain and Shiko Lake Cu-Au porphyry occurrences, central BC, over drift-covered sulphide-mineralized rock, and results indicated the CO_2 and O_2 variations were spatially coincident with inferred structures or mineralization beneath glacial deposits.

The prototype was modified after the initial testing to streamline the functionality, improve portability, and reduce potential contamination during measurements. The modified system was used at the Mount Milligan Mine property where a more robust survey was completed. The survey included measurements from 9 sites in 2020 and 154 sites in 2021 and benefit from a better understanding of the bedrock and surficial geology. Specifically, a subsequent trenching program provided direct observations to corroborate the soil gas survey results. The survey results showed good spatial correlations between soil gas CO_2 and O_2 anomalies and mapped bedrock fracturing in the trench. Additionally, $\Delta CO_2 \& O_2$ anomalies also correlated well with a projected fault trace on the southern part of the survey, with significant anomalies along the fault that could represent concentrated sulphide mineralization.

While the modified system has shown excellent potential for detecting bedrock faults and associated mineralization beneath drift covered areas, further testing is recommended to determine the efficacy of the system in thicker drift. In addition, it would be beneficial to understand and quantify the influence of soil moisture and composition on the measured gas concentrations, and what factors influence CO_2 and O_2 depth profile in the soil. Future improvements to the system could include an improved mechanism to better seal the probe in the soil, a backpack-style configuration for easier movement through survey areas and sensors to measure other gases. For example, CH_4 may be useful to discriminate between biogenic and geologic generated soil gas CO_2. The modified system has an option to mount a CH_4 sensor, but presently there is no circuit board or software available to process raw soil gas CH_4 data. Future studies should also consider evaluating the utility of real-time soil gas CO_2 and O_2 measurement systems for geothermal exploration, earthquake prediction and in agriculture research.

8. Acknowledgements

Funding for this project was provided by Geoscience BC and Centerra Gold Services Inc. W. Jackaman from Noble Exploration Services Ltd. kindly advised on an initial test of the system over the Leach River Fault zone north of Jordan River, and Haj Bains provided exceptional support in the field. Permission from K. Schimann, CanAlaska Uranium, to access the Mouse Mountain property is appreciated. R. Durfeld, Durfeld Geological Management Ltd. very kindly provided transportation from Williams Lake to the Shiko Lake property; advised on sample transect sites; and helped with the soil and soil gas measurements. His assistance and hospitality during the fieldwork was very much appreciated by the authors. J. Houck, CO2Meter Inc., is thanked for patiently and promptly answering many questions about the sensors. Altech machining and repairs Ltd, Victoria, BC, kindly assisted with machining parts for the soil gas collection probe. Centerra staff at the Mount Milligan mine are especially thanked for their support during the surveys in 2020 and 2021.

10. References

Abzalov, M.Z. (2008): Quality control of assay data: A review of procedures for measuring and monitoring precision and accuracy; Exploration and Mining Geology, v. 17, p. 1–14.

Amundson, R.G. and Davidson, E.A. (1990): Carbon dioxide and nitrogenous gases in the soil atmosphere; Journal of Geochemical Exploration, Vol. 38, p 13-41.

CO2Meter Inc. (2015): GSS sensor user manual; CO2Meter Inc., 51 p URL <http://www.co2meters.com/Documentation/Manuals/Manual-GSS-Sensors.pdf> [November 2019].

Cui, Y., Miller, D., Schiarizza, P., and Diakow, L.J., 2017. British Columbia digital geology. British Columbia Ministry of Energy, Mines and Petroleum Resources, British Columbia Geological Survey Open File 2017-8, 9p. Data version 2019-12-19.

Duddridge, G.A., Grainger, P. and Durrance, E.M. (1991): Fault detection using soil gas geochemistry; Quarterly Journal of Engineering Geology, v. 24, p. 427–435.

Dubé, B., Gosselin, P. Mercier-Langevin, P., Hannington, M., and Galley, A., 2007, Gold-rich volcanogenic massive sulphide deposits, *In* Goodfellow, W.D., ed., Mineral Deposits of Canada: A Synthesis of Major Deposit-Types, District Metallogeny, the Evolution of Geological Provinces, and Exploration Methods: Geological Association of Canada, Mineral Deposits Division, Special Publication No. 5, p. 75-94.

Fitzgerald, J., Jago, P.C., Jankovic, B.Sc. Geology, P.Geo. Simonian, B., Taylor, C.A., and Borntraeger. (2020): Technical report on the Mount Milligan mine, North-Central BC, Centerra Gold Inc. NI 43-101 Technical Report, 268 p.

Fletcher, W.K. (1981): Analytical methods in geochemical prospecting, Handbook of Exploration geochemistry Volume 1, Editor G.J.S Govett, 254 pp

Fridman, (1990): Application of naturally occurring gases as geochemical pathfinders in prospecting for endogenic deposits; Journal of Geochemical Exploration, Vol. 38, p 1-11.

Gingrich. J. E. (1984): Radon as a Geochemical Exploration Tool. Journal of Geochemical Exploration. Vol. 21, p. 19-39.

Hale, M. (2010): Gas geochemistry and deeply buried mineral deposits: the contribution of the Applied Geochemistry Research Group, Imperial College of Science and Technology, London; Geochemistry: Exploration, Environment, Analysis, v. 10, no. 3, p. 261–267.

Highsmith, P. (2004): Overview of soil gas theory; Explore, no. 122, p. 1–15.

Hodges, G., Kim, H., Brantley, S.L. and Kaye, J. (2019): Soil CO2 and O2 Concentrations illuminate the relative importance of weathering and respiration to seasonal soil gas fluctuations; Journal of the Soil Science Society of America, 83 p 1167–1180.

Jonnes, S. and Logan, J.M. (2007): Bedrock geology and mineral potential of Mouse Mountain, central British Columbia; in Geological Fieldwork 2006, BC Ministry of Energy, Mines and Petroleum Resources, BC Geological Survey, Paper 2007-1, p. 55–66, URL <http://cmscontent.nrs.gov.bc.ca/geoscience/PublicationCatalogue/Paper/BCGS_P2007-01-06_Jonnes.pdf> [November 2019].

Kesler, S.E., Gerdenich, M.J., Steininger, R.C., and Smith, C. (1990). Dispersion of soil gas around micron sized gold deposits; Journal of Geochemical Exploration 38, p 117-132.

Lesage, G. (2011): Assessment report on the Red gold property, Cariboo Mining Division, BC, NTS: 093A06W; BC Ministry of Energy, Mines and Petroleum Resources, Assessment Report Indexing System (ARIS), ARIS Report 32975, 755 p., URL <https://aris.empr.gov.bc.ca/ArisReports/32975.PDF> [November 2019].

Lett, R.E., Sacco, D.A., Elder, B. and Jackaman, W. (2020); Real-time analysis of soil gas for carbon dioxide and oxygen to identify bedrock mineralization and geological faults beneath glacial deposits in central British Columbia; Geoscience BC Report 2020-07, 50 p.

Logan, J.M., Schiarizza, P.A., Struik, L.C., Barnett, C., Nelson, J.L., Kowalczyk, P., Ferri, F., Mihalynuk, M.G., Thomas, M.D., Gammon, P., Lett, R.E., Jackaman, W., Ferbey, T (2010). Bedrock Geology of the QUEST Map Area, Central British Columbia, BCGS Geoscience Map 2010-01; GSC Open File 6476.

Lovell, J.S., Hale, M, and Webb, J.S. (1993). Soil air carbon dioxide and oxygen measurements as a guide to concealed mineralization in semi-arid and arid regions. Journal of geochemical exploration, 19, pp 305-317.

Lovell, J.S., Hale, M. and Webb, J.S. (1979): Soil air disequilibrium as a guide to concealed mineralization at Keel, Eire; in Prospecting in Areas of Glaciated Terrain, 1979: papers presented at a symposium organized by the Irish Association for Economic Geology and held in Dublin, Ireland, 26–29 August, 1979, The Institute of Mining and Metallurgy, London, p. 45–50.

Lovell, J.S., Hale, M. and Webb, J.S. (1980): Vapour geochemistry in mineral exploration; Mining Journal, 1990, p. 229–239.

Lucic, G., Stix, J., and Wing, B. (2015): Structural controls on the emission of magmatic carbon dioxide gas, Long Valley Caldera, USA; Journal of Geophysical Research: Solid Earth, 120, p 2262–2278.

McCarthy, J.H., Lambe, R.N. and Dietrich, J.A. (1986): A case study of soil gases as an exploration guide in glaciated terrain: Crandon massive sulfide deposit, Wisconsin; Economic Geology, v. 81, p. 408–420.

Morton, J.W. (2003): Prospecting and a geological reconnaissance on the Red gold property, Cariboo Mining Division, BC; BC Ministry of Energy, Mines and Petroleum Resources, Assessment Report Indexing System (ARIS), ARIS Report 27046, URL <https://aris.empr.gov.bc.ca/ArisReports/27046.PDF> [November 2019].

Robb, L., (2005): Introduction to ore forming processes, Blackwell, 368 p.

Rukhlov, A.S., Ootes, L., Hickin, A.S., and Mashyanov, N.R (2021): Near-surface mercury vapour haloes in air above ore deposits and faults on Vancouver Island: Insights into buried materials in real-time? In Geological Fieldwork 2020, B.C. Ministry of Energy, Mines and Petroleum Resources, Paper 2021-01 pp 130-143

Schimann, K. (2014): Geology and geochemistry at the QM property, NTS: 93G 01, BC; BC Ministry of Energy, Mines and Petroleum Resources, Assessment Report Indexing System (ARIS), ARIS Report 35262, 28 pp.

Smee, B.W. (1998): A new theory to explain the formation of soil geochemical response over deeply covered gold mineralization in arid environments; Journal of Geochemical Exploration, v. 61, p. 149–172.

Smee, B.W. (2003): Theory behind the use of soil pH measurements as an inexpensive guide to buried mineralization, with examples; Explore, no. 118, p. 1–18.

Smee, B.W. (2009): Soil micro-layer, airborne particles, and pH: the Govett connection; in Proceedings of the 24th International Applied Geochemistry Symposium, June 1–4, 2009, Fredericton, New Brunswick, Eds. D.R. Lentz, K.G. Thorne and K.-L. Beal, v. 1, p. 91–95.

Appendix A

Mount Milligan soil gas measurements

Provided separately as Developments in the real-time detection of buried mineralization and geological structures using soil gas_AppendixA.xlsx